Theor Chem Acc (2012) 131:1279
DOI 10.1007/s00214-012-1279-7

REGULAR ARTICLE

$O + C_2H_4$ potential energy surface: lowest-lying singlet at the multireference level

Aaron C. West · Joseph D. Lynch · Bernhard Sellner · Hans Lischka · William L. Hase · Theresa L. Windus

Received: 8 May 2012 / Accepted: 10 September 2012 / Published online: 10 October 2012

Abstract In previous studies (West et al. in J Phys Chem A 113(45):12663, 2009; West et al. in Theor Chem Acc 131:1123, 2012), the lowest-lying $O(^3P) + C_2H_4$ and singlet PES near the $\cdot CH_2CH_2O\cdot$ biradical were extensively explored at several levels of theory. In this work, the lowest-lying $O(^1D) + C_2H_4$ PES is further examined at the multiconfigurational self-consistent field (MCSCF), MRMP2, CR-CC(2,3), GVB-PP, and MR-AQCC levels. This study aims to provide a detailed comparison of these different levels of theory for this particular system. In particular, many reactions for this system involve multiple bond rearrangements and require various degrees of both non-dynamic and dynamic correlation for reasonable energetics. As a result of this variety, coupled cluster results parallel but do not always match up with multireference results as previously anticipated. In the case of the $CH_2CHOH \rightarrow$ oxirane pathway, MCSCF results show the possibility of a two-step mechanism rather than an elementary step, but the case is very difficult to elucidate. In the case of the $CH_3C{:}–OH \rightarrow H_2CCO + H_2$ pathway, a non-traditional NEB MEP at the GVB-PP level and MR-AQCC stationary point determination illustrate the need for a complex treatment of this surface.

Keywords CASSCF · MR-AQCC · MRMP2 · CR-CC(2,3) · Multireference · GVB-PP · Perfect pairing · IRC · Ketocarbene · Combustion

Electronic supplementary material The online version of this article (doi:10.1007/s00214-012-1279-7) contains supplementary material, which is available to authorized users.

A. C. West · T. L. Windus (✉)
Department of Chemistry, Iowa State University, Ames, IA 50011, USA
e-mail: twindus@iastate.edu

J. D. Lynch
Robert C. Byrd Health Sciences Center, School of Medicine, P.O. Box 9100, Morgantown, WV 26506-9600, USA

B. Sellner · H. Lischka
Institute for Theoretical Chemistry, University of Vienna, Waehringerstrasse 17, 1090 Vienna, Austria

B. Sellner
Chemical and Materials Sciences Division, Pacific Northwest National Laboratory, Richland, WA 99354, USA

H. Lischka · W. L. Hase
Department of Chemistry and Biochemistry, Texas Tech University, Memorial Circle and Boston, Lubbock, TX 79409-1061, USA

1 Introduction

For the O + ethylene system, both theoretical and experimental [1–5] studies strive toward more accurate potential energy surface (PES) methods, which could subsequently serve as a model to advance combustion studies on larger hydrocarbon systems [6]. Our previous work [1, 2] established that discerning transition states (TSs) and minimum energy paths (MEPs) for this system can sometimes be elusive at both the single reference and multireference levels.

Several initial theoretical studies [7–11] of the PES of this reaction were conducted, but the more recent PES studies of Nguyen et al. [12] and Yang et al. [13] gave more comprehensive surveys of the O + ethylene PES. Dynamics studies range from examining the dynamics in the $\cdot CH_2CH_2O\cdot$ biradical region in Hu et al. [14] to single-state dynamics studies of Joshi et al. [15] and Bowman et al. [16–18].

Our first study [1] on the lowest-lying triplet examined pathways 1–9 from Nguyen's [12] work with an additional triplet path 10, and our second study [2] analyzed excited states, surface crossings, and reactions near the $\cdot CH_2CH_2O\cdot$ and $\cdot CH_2\cdot CHOH$ biradicals. The current study adds to the previous paper [2] by examining the barriers farther from the $\cdot CH_2CH_2O\cdot$ biradical PES region: the lowest-lying singlet paths 14–19 and 21–25 as labeled in Nguyen et al. [12] at several levels of theory. This study examines the following reactions at multiple levels of theory.

14 $CH_3CHO \rightarrow CH_2CHOH$
15 $CH_3C{:}{-}OH \rightarrow CH_3CHO$
16 $CH_3C{:}{-}OH \rightarrow CH_2CHOH$
17 $CH_3CHO \rightarrow \cdot CH_3 + \cdot CHO$
18 $CH_3CHO \rightarrow CH_3\cdot CO + \cdot H$
19 $CH_3CHO \rightarrow \cdot CH_2CHO + \cdot H$
21 $CH_3CHO \rightarrow CH_4 + CO$
22 $CH_2CHOH \rightarrow$ oxirane
23 oxirane $\rightarrow CH_3OC{:}{-}H$
24 $CH_2CHOH \rightarrow H_2CCO + H_2$
25 $CH_3C{:}{-}OH \rightarrow H_2CCO + H_2$
26 oxirane $\rightarrow \cdot\cdot CH_2 + H_2CO$

2 Methods

Results from calculations at the MCSCF and MRMP2 levels in this paper were performed with the GAMESS software [19]. The multireference procedure from the previous work [1, 2] was used in the current work and is only summarized here. Multireference calculations were carried out at the complete active space self-consistent field (CASSCF) [20–29] level of theory with the aug-cc-pVTZ [30] basis set. The determinant-based method [31] and the full Newton–Raphson converger with augmented Hessian technique [32–34] were used to obtain solutions because of the large complete active space (CAS) sizes. Restricted Hartree–Fock (RHF) or restricted open-shell Hartree–Fock (ROHF) calculations with modified valence orbitals [35] and Boys localization [36] provided good starting orbitals for most pathways. In particular, the ROHF orbitals can provide good starting orbitals for open-shell singlets. CASSCF stationary point searches for species in the reactions above employed analytical gradients and central-differenced, numerical Hessians. Intrinsic reaction coordinate (IRC) runs were obtained with the second-order Gonzalez-Schlegel (GS2) method [37] to identify the minima associated with TSs. If an elementary reaction involves a single bond break with no TS, a series of constrained optimizations at the CASSCF level were performed to a bimolecular distance of about 5 Å, which was further optimized without constraint as a supermolecule to a bimolecular geometry. The individual pathway sections list any imaginary frequencies present at any bimolecular stationary points with or without a TS in the elementary step.

Once a reaction path was located, second-order single-state multireference Møller-Plesset perturbation (MRMP2) [38] single-point energies using the aug-cc-pVTZ [30] basis set were performed along the entire IRC to recover the majority of the dynamic correlation. From the previous work on the triplet surface, MRMP2 results quantitatively agreed with multireference average quadratic coupled cluster (MR-AQCC) [39] results using COLUMBUS [40–42]. However, previous work [2] on the singlet revealed that this chemical system requires substantial dynamic correlation for some pathways. So the following additional calculations were performed.

Completely renormalized coupled cluster singles, doubles, and non-iterative triples CR-CC(2,3) [43, 44] single-point energies with aug-cc-pVDZ [30] and aug-cc-pVTZ [30] basis sets were also performed for all paths along the IRC (or constrained optimization series) except for 14, 22, and 25. In difficult cases, the ROHF reference was used instead of the RHF reference. For path 14 the GS2 CASSCF IRC calculation failed, and orbital root flipping (ORF—when an orbital not originally in the active space "flips" into the active space) precluded one side of the IRC. So only stationary points were used in path 14 calculations. Paths 22 and 25 require a more careful examination.

Paths 22 and 25 are examples of particularly difficult portions of the PES. So the generalized valence bond–perfect pairing (GVB-PP) [45–47] approach for the wave function was utilized using COLUMBUS [40–42] for these calculations. For path 25 only, additional MR-AQCC calculations were performed. For the GVB-PP calculations, 9 pairs are used with each pair consisting of two electrons in two orbitals—GVB-PP(9). Besides the chemical core O 1s and C 1s orbitals, which are doubly occupied, all other orbitals are treated on an equal footing allowing for the correct dissociation of individual electron pairs. The total electronic wave function consists of an antisymmetrized product of the nine perfect pairs yielding a space of 2^9 (512) configurations. At the GVB-PP level, all stationary points of the reaction were characterized by frequency calculations using both the cc-pVDZ [30] and cc-pVTZ [30] basis sets.

On top of the GVB-PP(9)/cc-pVDZ level geometries, a MR-AQCC PP(6) study on path 25 was performed. All pairs are active in the reference space except two non-action CH bonds and the CC σ bond, which are doubly occupied, and their weakly occupied antibonding orbitals in the virtual space. Here and throughout this paper, "action" coordinates refer to internal coordinates that significantly change in length or degree relative to

remaining (i.e. "non-action") internal coordinate changes, which are defined by cutoffs. Based on this reference space, single and double excitations are allowed imposing generalized interacting space restrictions [48], which results in an MR-AQCC expansion space of 6,109,120 configurations. At this level, all stationary points of path 25 were characterized by frequency calculations using the cc-pVDZ [30] basis set. Hessians were computed with the program Suscal [49] by means of finite differences using analytic gradients [50–52].

The MEP was computed using the nudged elastic band (NEB) method [53–56] for pathway 25 and the traditional IRC method [57–59] for pathway 22 as implemented in MEPPACK (part of COLUMBUS; for more details, see Sellner [60]) at the GVB-PP(9)/cc-pVDZ level. The Hessian matrices used in the relaxation of these NEBs were approximated by scaled diagonal matrices. The convergence threshold on the root-mean-square (RMS) value of the modified gradient on each image in case of the path 25 NEB calculation is 10^{-3} aJ/(Å sqrt(amu)) and on the RMS value of the projected gradient in each step of the path 22 IRC calculation is 10^{-4} aJ/(Å sqrt(amu)).

3 Results and discussion

Table 1 displays the active space for each reaction where the labels "near" and "far" refer to the carbon closest and farthest from oxygen, respectively. Examination of bond length changes, natural orbital occupation numbers, and localized molecular orbital coefficients over the course of each reaction in different CAS sizes ultimately decide the choice of active space. As described in the previous papers [1, 2], results with in–out correlation (IOC—a mostly unoccupied orbital that has an additional, inappropriate radial node) usually result in ORF. So unless either the IOC constitutes proper radial correlation at some geometry in the pathway or ORF prevents placing the lone O2p in the MCSCF core, CASSCF active spaces do not contain IOC orbitals. However, as will be shown, current, variational techniques do not always allow for chemically intuitive active spaces to persist in many reaction pathways.

Tables 2 and 3 give the overall barrier information for all elementary reactions (except for the multistep reaction 25) whereby each TS divides each pathway into reactant to TS (forward barrier) and product to TS (reverse barrier). Table 2 shows the CAS barriers with and without zero-point energies (ZPE), and Table 3 gives the barriers from MRMP2 energies at the CAS stationary points (stationary point MRMP2—SPMRMP2), CR-CC(2,3) optimized geometries at the aug-cc-pVDZ [30] basis, Nguyen et al. [12] and Yang et al. [13] barriers, and single-point MRMP2 and CR-CC(2,3) energies at the CASSCF TS geometry and IRC endpoint geometries (i.e. "select" geometries). While the single-point MRMP2 barriers are not strictly barriers of optimized structures, they should be approximately representative of them as previously shown [1]. In addition, for these particular pathways, SPMRMP2 energy barriers always include ZPE (except for species with ORF issues in numerical Hessians as discussed below). Table 4 gives barriers for the GVB-PP and existing MR-AQCC calculations. The natural orbital configuration interaction (NOCI) coefficients help to suggest multireference character. So, in difficult cases, this additional analysis is given. Since no absolute cutoff exists to indicate a multireference situation based on the size of the squared NOCI coefficients, two approximate indicators are chosen for this study. First, if the dominant NOCI weight (i.e. the square of the largest NOCI coefficient) is below 0.95, this approximate cutoff strongly suggests that (dynamical or quasi-degenerate) correlation plays an important role. Paths 14, 21, and 25 each show the dominant NOCI weight below 0.95. Second, if any NOCI weights other than the dominant NOCI weight are above 0.05, this approximate cutoff suggests a multireference situation with quasi-degenerate correlation. Paths 21 and 25 show additional weights above 0.05. Such an analysis might suggest when the CR-CC(2,3) energies are inappropriate. However, even when the above analysis does not suggest multireference character and the reaction of interest simultaneously involves multiple bond rearrangements, borderline cases are possible.

For the rest of the results in this section, specifics on each of the reactions are presented and discussed. Unless otherwise explicitly noted, the descriptions contain the following: barriers and energetics comparisons include ZPE; "select" barriers are calculated using the select geometries without ZPE; the CASSCF active spaces do not contain IOC and contain one lone O2p orbital in the MCSCF core; any references made to stationary points refer to CASSCF stationary points (except for explicitly denoted GVB-PP, MR-AQCC, or CR-CC(2,3) optimizations); basis set energy differences are given from the aug-cc-pVDZ [30] to the aug-cc-pVTZ [30] basis at the CR-CC(2,3) level of theory without ZPE at select geometries (as specified in Table 3) and are reported only when the difference exceeds 1.0 kcal/mol; CR-CC(2,3) select barriers are reported with the aug-cc-pVTZ basis in the text; and individual pathways report only non-negligible geometry changes in this study's CASSCF stationary points relative to Nguyen's [12] B3LYP results.

3.1 Pathway 14: $CH_3CHO \rightarrow CH_2CHOH$

In this reaction a hydrogen shifts from the carbon farthest from the oxygen to the oxygen itself. The involvement of the oxygen here in multiple bond changes (e.g. the transformation of a CO π, π^* to a CC π, π^*) requires three O2p orbitals in the active space and leads to IOC, which

Table 1 Description of the main CAS sizes used for each reaction pathway

Reaction pathway	Active space	In–out correlation	Description
14	(14,14)	Y	3 CHσ, COπ, COσ, CCσ, lone O2p
			→2 CHσ, CCπ, OHσ, COσ, CCσ, lone O2p
15	(8,8)	Y	COσ, COπ, OHσ, lone C2p
			→ COσ, COπ, CHσ, lone O2p
16	(10,10)	N	CCσ, 3 CHσ, lone C2p
			→ CCσ, 3 CHσ, CCπ
	(14,14)	Y	COσ, CCσ, 3 CHσ, lone C2p, lone O2p
			→ COσ, CCσ, 3 CHσ, CCπ, lone O2p
17	(8,8)	Y	COπ, lone O2p, COσ, CCσ
			→ 2 COπ, COσ, biradical(near C2p;O2p, far C2p)
18	(8,8)	Y	COπ, lone O2p, COσ, CHσ
			→ 2 COπ, COσ, biradical(near C2p;O2p, H)
19	(12,12)	N	3 CHσ, COπ, COσ, CCσ
			→ 2 CHσ, COπ, COσ, CCσ, biradical(far C2p, H)
21	(10,10)	Y	Near CHσ, COπ, loneO2p, COσ, CCσ
			→ far CHσ, COπ, COπ, COσ, CCσ
22 Step 1	(6,6)	N	Far CHσ, CCσ, CCπ
			→ near CHσ, CCσ, lone C2p, lone C2 s
22 Step 2	(10,10)	Y	OHσ, CCσ, COσ, lone C2p,lone O2p
			→ CHσ, CCσ, 2COσ, lone O2p
23	(10,10)	Y	CHσ, CCσ, 2COσ, lone O2p
			→ CHσ, lone C2p, 2COσ, COπ
24	(10,10)	Y	CHσ, OHσ, loneO2p, CCπ, COσ
			→ HHσ, 2 COπ, CCπ, COσ
26	(6,6)	N	CCσ, 2COσ
			→ COσ, COπ, biradical(far C2p, far C2 s)

Only the lone pairs and bonding orbitals are shown; the antibonding orbitals can be inferred from bonding orbitals and the indication of in–out correlation. The O2 s is always in the core

requires the use of an even (14,14) CAS. Both minima are A′ states with C_s symmetry while the TS is asymmetric. Despite the presence of both a reasonable active space and frequencies at the TS, the GS2 computation resulted in an excess of constrained optimizations on the hypersphere surface in an attempt to reach the next point in the IRC. In addition, the vinyl alcohol ends up with a carbon–carbon IOC orbital instead of an O2p* IOC orbital in the CAS. Therefore, an IRC is unavailable for this pathway.

The CR-CC(2,3) TS optimization failed while CR-CC(2,3) select barriers do not even match any other results to within ~10.0 kcal/mol. Because of this failure, further analysis is required in terms of weights (as previously described). At the CASSCF TS geometry, the dominant NOCI weight is 0.90 with no other weights above the approximate 0.05 cutoff, and the coupled cluster T2 amplitude magnitudes are small (i.e. |amplitude| <0.1 as the cutoff). However, as stated above, this reaction simultaneously involves multiple bond changes which suggests that multireference character may be playing a role. The forward (reverse) barrier is 68.1 (57.1) kcal/mol at the SPMRMP2 level. Because of the carbon–carbon IOC orbital on vinyl alcohol, the reverse barrier could be less accurate than the forward barrier. In addition, vinyl alcohol has two possible conformations with C_s symmetry because of OH rotation, which gives an energy difference of only ~1 kcal/mol at the CASSCF level. Since an IRC for a different reaction with a smaller CAS space leads to the higher energy conformer, the enthalpy was calculated with the higher energy conformer. Experimental results show the overall reaction enthalpy to be 9.9 kcal/mol [61, 62], which closely matches 11.0 (11.3) kcal/mol derived from SPMRMP2 (CR-CC(2,3) optimization) for this path. Furthermore, these results also match Nguyen and Yang results to within 1.0 kcal/mol.

3.2 Pathway 15: CH_3C:–OH → CH_3CHO

For this pathway an (8,8) CAS models a hydrogen shift from 1-hydroxyethylidene to acetaldehyde. In this case, the IRC has C_s symmetry. Despite several attempts at a (6,6) and an (8,7) CAS, this pathway unfortunately required an IOC orbital in order to avoid ORF. Dynamic correlation from MRMP2 leads to a modest shift in pathway energetics and essentially no shift along the reaction coordinate. Here and throughout this paper, a shift simply refers to how single-point energies at a different level of theory horizontally and vertically change the IRC curvature. The forward barrier (reverse barrier) is 23.3 (78.2) kcal/mol at the SPMRMP2 level, and with CR-CC(2,3) optimized geometries, the forward (reverse) barrier is 29.3 (78.6) kcal/mol. Nguyen, Yang, and the CR-CC(2,3) barriers all match to within 1 kcal/mol.

3.3 Pathway 16: CH_3C:–OH → CH_2CHOH

The reaction for 1-hydroxyethylidene to vinyl alcohol requires at least a (10,10) CAS. In addition, a (14,14) CAS provides some additional comparisons for this pathway. The (14,14) CAS has IOC whereas the (10,10) CAS has a

Table 2 Barriers to reactions in kcal/mol calculated at the CAS level without and with (in parenthesis) ZPE

Reaction pathway	CAS forward barrier[a]	CAS reverse barrier[a]	Nguyen's forward barrier[b]	Nguyen's reverse barrier[b]
14	80.1	51.2	67.6	56.9
	(76.8)	(47.4)		
15	34.2	90.9	28.4	79.4
	(30.4)	(87.2)		
16[c]	27.0	72.0	23.2	63.5
	(24.6)	(69.1)		
16[d]	29.6	70.1		
	(27.0)	(67.2)		
17	76.7	N/A	82.0	N/A
	(68.9)	(N/A)		
18	85.5	N/A	87.3	N/A
	(78.0)	(N/A)		
19	92.7	N/A	93.8	N/A
	(84.6)	(N/A)		
21	88.1	102.5	83.4	89.3
	(83.6)	(101.7)		
22 step 1	81.7	1.4	N/A	N/A
	(79.1)	(0.7)		
22 step 2	12.4	79.0	N/A	N/A
	(10.7)	(75.4)		
23	82.2	39.0	75.8	35.9
	(78.5)	(37.2)		
24	100.3	83.4	85.6	70.6
	(94.3)	(86.8)		
26	3.6	70.1	N/A	N/A
	(4.6)	(65.0)		

Nguyen's barriers include ZPE

[a] CAS barriers are obtained from unconstrained optimizations of intermediates and ~3–5 Å separated products

[b] Nguyen's [12] barriers are the average barriers from several different levels of theory

[c] (10,10) CAS

[d] (14,14) CAS

core O2p (i.e. no IOC). Here, both minima have C_s symmetry while the rest of the pathway has no symmetry. For the (10,10) CAS with the lower energy vinyl alcohol conformer as an endpoint, the forward barrier (reverse barrier) is 19.0 (62.7) kcal/mol at the SPMRMP2 level. For the reverse barrier in the (14,14) CAS, the IRC converges to the vinyl alcohol minimum with a rotated hydroxyl group in a higher energy conformation; but just as in path 14, the rotation makes little difference to the reverse barrier. Based on the CR-CC(2,3) data, the basis set energy difference is approximately 1.1 kcal/mol. The CR-CC(2,3) TS optimization failed. The CR-CC(2,3) select forward (reverse) barrier is 25.0 (64.4) kcal/mol. Here, the select barriers involve the higher energy vinyl alcohol conformer. These results match Nguyen and Yang forward barrier to within 2 kcal/mol. The T2 amplitude magnitudes are below the cutoff, and the dominant NOCI weight is 0.93.

For geometry comparisons, (10,10) and (14,14) CAS geometries are very similar. The CC bond length goes from 1.53 to 1.41 Å in the forward barrier and from 1.41 to 1.35 Å in the reverse barrier. The TS geometry has action CCH angles of 60° and 56°. In the forward barrier, the CO distance slightly changes from 1.30 to 1.35 Å.

3.4 Pathway 17: $CH_3CHO \rightarrow \cdot CH_3 + \cdot CHO$

This pathway is the first of three barrierless, acetaldehyde dissociations that require both constrained optimizations and a basis larger than a double zeta basis. Here, barrierless means that there is no maximum in the PES before dissociation. For this pathway an (8,8) CAS provides a qualitatively reasonable wave function for breaking the carbon–carbon bond plus accompanying bonding changes. From previous calculations with the analogous triplet pathway [1], it is well known that the active space must contain all three O2p orbitals. Since ORF occurs for a pure (i.e. not state-averaged) state (8,7) CAS, the calculations must include IOC. The results for this pathway are all in the A′ state in C_s symmetry. Since this pathway has no TS, energy differences between minima are given.

First, based on the CR-CC(2,3) select barriers, this pathway displays a 4.2 kcal/mol basis set energy difference. So, a double zeta basis would be insufficient to describe the energetics to within 1 kcal/mol. Second, at the SPMRMP2 level, this separation requires 74.6 kcal/mol. The 5 Å fragment (not a CASSCF minimum within the constraints of the constrained optimization) has one imaginary frequency of $26i$ cm^{-1} at the CASSCF level that points along the motion of the two products leaving each other (along the line of symmetry). Extending the distance to ~10 Å, the supermolecule energy only differs by ~1 kcal/mol from the 5 Å supermolecule energy. Third, at the CR-CC(2,3)/aug-cc-pVDZ level, supermolecule geometry optimizations led to an energy difference of 84.4 kcal/mol at 5 Å distance while optimizations on the individual doublet CH_3 and CHO products and singlet acetaldehyde yielded differences of 85.8 kcal/mol (without ZPE) and 77.9 kcal/mol (with ZPE). More strictly, comparing select MRMP2 and CR-CC(2,3) energies confirms the particular importance of dynamic correlation for accurate energetics in this pathway. Comparing the supermolecule and doublet optimized energetics shows the large contribution to the dynamic correlation derives from interactions from the CC σ, σ^* bonds. In fact, at the 5 Å supermolecule, T2 amplitude magnitudes at or above the

Table 3 Barriers to reactions in kcal/mol from single-point energies calculated at the MRMP2 level with aug-cc-pVTZ, and CR-CC(2,3) level with both aug-cc-pVDZ (ACCD) and aug-cc-pVTZ

Reaction pathway	SPMRMP2[a] (ZPE)	Opt CR-CC(2,3) (ZPE) (ACCD)	Nguyen[b]/Yang (ZPE)	Opt CR-CC(2,3) (ACCD)	Select MRMP2	Select CR-CC(2,3)	Select CR-CC(2,3) (ACCD)
14 R	57.1	–	56.9 56.4[d]	–	60.9[f]	70.5[f]	71.0[f]
14 F	68.1	–	67.6 67.0[d]	–	71.4[f]	59.6[f]	59.0[f]
15 R	78.2	78.6	79.4 79.3[d]	82.6	81.9	82.5	82.7
15 F	23.3	29.3	28.4 28.7[d]	33.0	27.0	32.3	32.9
16 R[i]	62.7	–	63.5 62.4[d]	–	64.7	64.4	63.3
16 F[i]	19.0	–	23.2 23.7[d]	–	21.4	25.0	25.4
16 R[j]	61.2	–	–	–	64.1	–	–
16 F[j]	19.5	–	–	–	22.1	–	–
17	74.6	84.4 77.9[g]	82.0	92.0 85.8 [g]	82.4	96.6	92.4
18	83.5	86.8 83.6[g,h]	87.3	94.3 91.2[g,h]	91.0	97.8	94.4
19	88.6	– 90.3[g,h]	93.8	– 98.3[g,h]	96.7	103.8	99.9
21 R	84.7	90.8 91.1[g]	89.3	91.9 91.7[g]	85.6	91.6	92.5
21 F	76.9	82.5	83.4	86.8	80.1	86.9	86.5
22 S1 R[k]	– 4.1	–	–	–	−3.4	−3.1	−2.6
22 S1 F[k]	77.7	–	–	–	80.3	76.4	74.5
22 S2 R[k]	68.0	–	–	–	71.6	72.2	70.3
22 S2 F[k]	– 1.3	–	–	–	0.4	3.4	5.0
23 R	27.1 29.0[c]	–	35.9 32.1[d]	–	28.9	32.6	33.3
23 F	74.9 76.8[c]	–	75.8 74.9[d]	–	78.5	77.9	76.4
24 R	68.3	68.2	70.6	66.0	65.3	65.9	65.7
24 F	84.4	85.6	85.6	91.8	89.6	90.3	90.6
26	81.4	– 79.6[g]	85.7	– 88.5 [g]	91.6	89.9	85.3

F indicates the forward barrier while R indicates the reverse barrier. SPMRMP2 barriers include ZPE from CASSCF stationary points. Nguyen's barriers include ZPE. Select MRMP2 and CR-CC(2,3) barriers do not include ZPE and are all at the same CASSCF geometries. In addition, energy differences with and without CR-CC(2,3) ZPE are given for geometry optimizations at the CR-CC(2,3) level with an aug-cc-pVDZ basis

[a] SPMRMP2 values derive from CAS stationary points, which are obtained from unconstrained optimizations of intermediates and ~ 3-5 Å separated products

[b] Nguyen's [12] barriers are the average barriers from several different levels of theory and are unlabeled in the column

[c] MRMP2 barrier with ZPE from shifts in the TS only

[d] Yang's [13] barriers at the CCSD(T)/cc-pVTZ//B3LYP/6-311++G* level of theory

[e] ORF indicates orbital root flipping

[f] Single-point energies performed at CASSCF stationary points rather than off of IRC

[g] Optimizations separately performed on each product fragment

[h] Energy value for doublet hydrogen is taken from ROHF as -0.4993343154 Hartree

[i] (10,10) CAS

[j] (14,14) CAS

[k] "S" indicates step for the two pseudo-elementary steps located for pathway 22

Table 4 Barriers to reactions in kcal/mol calculated at the GVB-PP level without and with (in parenthesis) ZPE at the cc-pVDZ or cc-pVTZ basis as labeled

Reaction pathway	GVB-PP forward barrier[a]	GVB-PP reverse barrier[a]	Nguyen's forward barrier[b]	Nguyen's reverse barrier[b]
22 S1[d,e]	77.0	8.0	N/A	N/A
	(74.4)	(7.5)		
22 S2[d,e]	29.4	82.5	N/A	N/A
	(28.6)	(78.8)		
25	51.8[f]	N/A	33.0	58.3
	(46.6)[f]	(N/A)		
	[33.0][c,e]	[N/A]		

Path 25 also includes barriers with MR-AQCC optimized geometries at the cc-pVDZ basis with ZPE in square brackets; as described in the text, the TS geometry with the most reasonable geometry is used in the construction of path 25 barriers. Nguyen's barriers include ZPE

[a] GVB-PP barriers from GVB-PP stationary points

[b] Nguyen's [12] barriers are the average barriers from several different levels of theory

[c] MR-AQCC barrier from MR-AQCC stationary points

[d] "S" indicates step for the two pseudo-elementary steps located for pathway 22

[e] cc-pVDZ basis

[f] cc-pVTZ basis

0.1 cutoff are on the orders of 0.75 and 0.1, which indicate strong multireference character.

The 5 Å CR-CC(2,3), 84.4 kcal/mol energy difference matches the experimental result of 84.8 kcal/mol [63] and Nguyen energetics of 82.0 kcal/mol. With respect to the SPMRMP2 energetics, IOC in the wave function might slightly contribute to the 10.2 kcal/mol error in the final energetics. In terms of energy differences with respect to differing geometries, the individual coupled cluster geometries differ by very little from the corresponding geometries in a 5 Å supermolecule. Given the difference in the basis set energies and the computationally expensive CR-CC(2,3) optimizations with a triple zeta basis, these coupled cluster calculations give the barrier to be ~75.2–80.6 kcal/mol, which matches the MRMP2 results just as well as the experimental barrier. It should also be noted that while there are large energy barriers in these reactions, they will be favored by entropy since they lead to multiple products.

3.5 Pathway 18: $CH_3CHO \rightarrow CH_3{\cdot}CO + {\cdot}H$

This hydrogen dissociation also requires constrained optimizations in C_s symmetry with an (8,8) CAS that contains IOC; modeling this pathway involves the same issues as modeling pathway 17. The basis set energy difference is 3.4 kcal/mol, which is again quite large. At the ~5 Å product, two imaginary frequencies are still present for the CASSCF, constrained stationary point. The first imaginary frequency of $34i$ cm^{-1} points from the hydrogen fragment along the motion of the two fragments leaving each other (along the line of symmetry). The second imaginary frequency of $33i$ cm^{-1} involves a methyl rotation and a bend of the CO group out of the plane. In addition, the CR-CC(2,3)/aug-cc-pVDZ level, supermolecule geometry optimizations (again, with two small imaginary frequencies) led to an energy difference of 86.8 kcal/mol, and the CR-CC(2,3)/aug-cc-pVDZ level, doublet optimizations led to an energy difference of 91.2 kcal/mol (without ZPE) and 83.6 kcal/mol (with ZPE).

As a result, the separation requires 83.5 kcal/mol at the SPMRMP2 level while the CR-C(2,3)/aug-cc-pVDZ supermolecule energy difference of 86.8 kcal/mol more closely matches Nguyen energy difference of 87.3 kcal/mol and the experimental barrier of 89.3 kcal/mol [61, 64, 65]. Again, these MRMP2 calculations did not recover enough dynamic correlation to get the energetics correct for this bimolecular reaction while the CR-CC(2,3) calculations may have issues due to the multireference character of the wave function. Besides the dissociating hydrogen, no major geometry changes take place in this pathway.

3.6 Pathway 19: $CH_3CHO \rightarrow {\cdot}CH_2CHO + {\cdot}H$

This hydrogen dissociation is the last barrierless pathway that was calculated with constrained optimizations. With a basis set energy difference of 3.9 kcal/mol, a larger than double zeta basis is again required for this pathway. Our previous paper [1] gives this dissociation on the triplet surface. The triplet dissociation is extremely problematic both with and without IOC; only an active space of three O2p orbitals and no IOC could lead to a smooth IRC. However, as before, (N,N-1) pure state, non-full valence, active spaces are not feasible with current convergers and still lead to ORF. Thus, for the singlet dissociation, the MCSCF core contains a lone O2p with the understanding that this CAS will lead to the least convergence issues in the search for pure states in this constrained optimization series. This pathway requires at least a (12,12) CAS and is asymmetric except at acetaldehyde, for which the calculations do not use symmetry. Pulling the fragments out to ~5 Å yields a separation energy of 88.6 kcal/mol at the SPMRMP2 level. CC-CR(2,3) optimized geometries result in energy differences of 90.3 kcal/mol for fully separated doublet products. CR-CC(2,3) supermolecular optimizations yielded diverging energies and were not pursued further. These results differ from Nguyen's energetics of 93.8 kcal/mol by 3.5 kcal/mol. In fact, relative to the Nguyen values, the CR-CC(2,3) select energy difference is larger at 103.8 kcal/mol.

3.7 Pathway 21: $CH_3CHO \rightarrow CH_4 + :CO$

This pathway from acetaldehyde also requires a compromised CAS because of computational expense. A (10,10) CAS with IOC starts with and retains acetaldehyde's methyl group in the MCSCF core rather than an active space that additionally contains the methyl group (i.e. compromised CAS). The reaction ultimately results in methane and carbon monoxide bimolecular fragments. For this pathway both acetaldehyde and ~ 5 Å bimolecular fragment calculations have an A′ state in C_s symmetry; so this pathway's IRC appears to be entirely symmetric with the given CAS size. However, the symmetric fragment geometry contains a small imaginary frequency of $22i$ cm^{-1} that essentially rotates the entire methane. Without this symmetry restriction on the bimolecular fragments, an ORF occurs so that all methane CH σ orbitals equivalently reside in the core. The forward (reverse) barrier is 76.9 (84.7) kcal/mol at the SPMRMP2 level. CR-CC(2,3) optimized geometries result in a forward (reverse) barrier of 82.5 (90.8) kcal/mol. However, the dominant CASSCF TS NOCI weight is 0.87 while another weight is 0.07, which indicates the correlation is important. In addition, the occupation number also suggests multireference character with a value of 0.17. Furthermore, the CR-CC(2,3) optimized doublets demonstrate that further separation comprises less than 1 kcal/mol contribution to the reverse barrier. The reaction enthalpy of $-7.8(-8.3)$ kcal/mol at the SPMRMP2 (CR-CC(2,3)/aug-cc-p-VDZ supermolecule) level differs from the experimental reaction enthalpy of -14.5 kcal/mol [61, 66]. Because of the CR-CC(2,3) results, this difference from experiment most likely does not derive from the use of the compromised CAS. Nguyen's forward and reverse barriers both lie within 2 kcal/mol of the corresponding CR-CC(2,3) results.

The OCC angle changes from 125° to 107° in the course of the forward barrier. The CC σ bond breaks in the forward barrier; and the CC distance changes from 1.53 to 2.22 Å. For the TS this study gives the distance from the action H to the carbon of methyl as 1.89 Å while Nguyen's study gives 1.73 Å; as well, this study finds the TS CC distance as 2.22 Å while Nguyen shows it to be 2.10 Å.

3.8 Pathway 22: $CH_2CHOH \rightarrow$ oxirane

Nguyen et al. reported this rearrangement as a concerted reaction. However, Yang et al. [13] indicated that at the CCSD(T)/cc-pVTZ//B3LYP/6-311++G* level, this pathway does not exist and in fact requires two steps: $CH_2CHOH \rightarrow HC{:}–CH_2OH$ and $HC{:}–CH_2OH \rightarrow$ oxirane. This reaction involves multiple bond formations and multiple numbers of lone pairs (i.e. O2p, C2p). In addition, the CR-CC(2,3) TS optimization also failed, which again suggests difficulties with this level of theory for multiple bond rearrangements. All attempts to find a one-step mechanism failed. However, in order to obtain energetics for the desired intermediates for the total reaction, GVB-PP geometry optimizations started with Nguyen's reported stationary points and produced corresponding extrema. GVB-PP gives the overall reaction with an enthalpy of 18.2 kcal/mol, which matches 17.2 kcal/mol from experiment [62, 66]. In an attempt to clarify the elementary steps for this reaction, various CAS sizes were used, but this study only reports results for non-ORF CAS and GVB-PP results below.

3.9 Pathway 22 Step 1: $CH_2CHOH \rightarrow HC{:}–CH_2OH$

Locating an IRC at the density function theory level with the hybrid B3LYP [67, 68] functional and the 6-31G* [69, 70] basis provided reasonable initial geometries for CASSCF geometry searches. Then, plotting CR-CC(2,3) and (6,6) CAS single-point energies along the DFT IRC reveals a particular difference in the elongated curvature (see Fig. 1): the larger barrier does not exist in the CASSCF curve unlike the single reference DFT and CR-CC(2,3).

In order to properly model this hydrogen transfer, a small, compromised (6,6) CAS size is required. Even though a possibly more chemically intuitive, larger CAS size is computationally feasible in this case, ORF occurs during the course of the IRC. At the beginning of this IRC, the active space minimally includes the CC and CH σ spaces and the CC π space. Figure 2 shows the CASSCF IRC with the MRMP2 and CR-CC(2,3) single-point energies. The $HC{:}–CH_2OH$ endpoint of the CASSCF IRC roughly corresponds to the end of the first barrier shown in the DFT IRC (Fig. 1) (around s = -2 bohr sqrt(amu)).

Based on the CR-CC(2,3) data, the basis set energy difference is approximately 1.9 kcal/mol. The GVB-PP(9)/cc-pVDZ IRC forward (reverse) barrier is 74.4 (7.5) kcal/mol, the (6,6) CAS IRC forward (reverse) barrier is 79.1 (0.7) kcal/mol, the forward (reverse) barrier is 77.7 (-4.1) kcal/mol at the SPMRMP2 level, and the CR-CC(2,3) select forward (reverse) barrier is 76.4 (-3.1) kcal/mol. Because of the curvature differences between DFT, CR-CC(2,3), and (6,6) CAS in Fig. 1, CR-CC(2,3) TS optimizations were not attempted. It is important to note that both the SPMRMP2 and CR-CC(2,3) results suggest that adding dynamic correlation makes this barrier disappear.

3.10 Pathway 22 Step 2: $HC{:}–CH_2OH \rightarrow$ oxirane

For the second step, a compromised (10,10) CAS is used for modeling. In particular, on the reactant side of step 2,

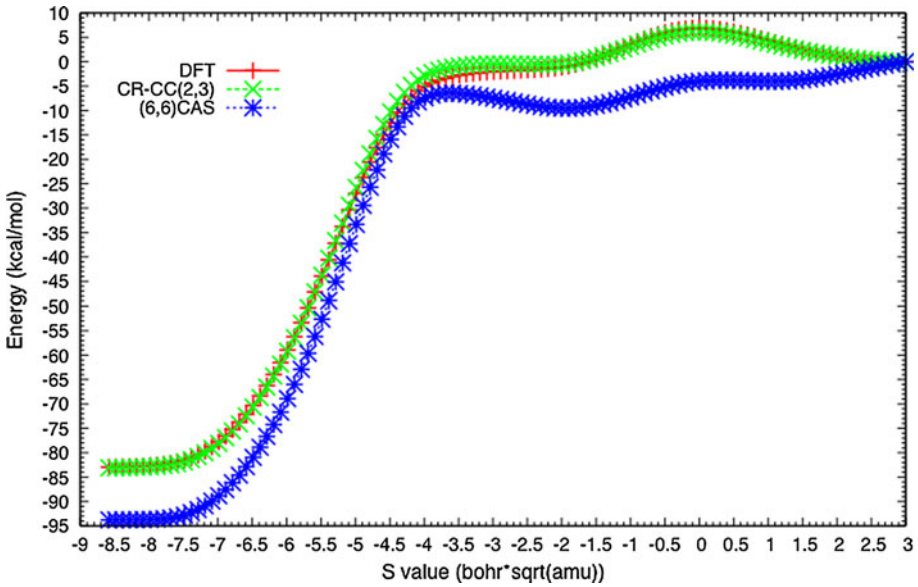

Fig. 1 Path 22 Step 1: DFT IRC and single-point energies (6-31G* basis no ZPE)

the 3 non-action CH σ orbitals are left out of the active space. Figure 3 shows the CASSCF IRC with the MRMP2 and CR-CC(2,3) single-point energies. Both the MRMP2 and CR-CC(2,3) methods lower the barriers relative to the CASSCF method. The HC:–CH_2OH endpoint of the CASSCF IRC is not the same as the one for step 2 and involves rotation of the O–C–C–H and C–C–O–H dihedrals. By performing a scan between these two points at the CASSCF (SPMRMP2) level, the step 2 endpoint is $\sim$6.6 (7.1) kcal/mol uphill in energy from the step 1 endpoint without an explicit barrier.

Based on the CR-CC(2,3) data, the basis set energy difference is again approximately 1.9 kcal/mol. The GVB-PP(9)/cc-pVDZ IRC forward (reverse) barrier is 28.6 (78.8) kcal/mol, the (10,10) CAS forward (reverse) barrier is 10.7 (75.4) kcal/mol, the forward (reverse) barrier is -1.3 (68.0) kcal/mol at the SPMRMP2 level, and the CR-CC(2,3) select forward (reverse) barrier is 3.4 (72.2) kcal/mol. The large GVB-PP forward barrier relative to the CAS and SPMRMP2 barriers most likely occurs since GVB-PP does not include the majority of the quasi-degenerate correlation for this step, which involves action among several more bonds than even in the reverse barrier for path 22 step 1. So while the CASSCF level shows two barriers (Figs. 2, 3), the CR-CC(2,3) and SPMRMP2 data suggest that the overall reaction (i.e. pathway 22) is one high-energy barrier with a very flat, extended surface (Figs. 2, 3 combined) that may or may not involve two steps.

3.11 Pathway 23: oxirane $\rightarrow$ CH_3OC:–H

This pathway depicts the ring-opening of oxirane and a hydrogen shift as concerted processes. As such, this compromised (10,10) CAS keeps 3 CH σ orbitals in the core and has IOC; this active space choice does not allow C_s symmetry for oxirane. As well, symmetric A′ calculations on CH_3OC:–H were not attempted because of previous difficulties with compromised CAS starting orbitals. Various attempts to place an O2p into the core (and hence allow for more CH σ, σ^* oribtals in the CAS) fail because the O2p enters the active space once the IRC reaches the CH_3OC:–H intermediate. Although this pathway has two closed-shell endpoints, it differs from other "closed-shell" pathways in the fact that dynamic correlation slightly shifts the TS along the reaction coordinate; the minima only energetically shift. The forward barrier (reverse barrier) is 74.9 (27.1) kcal/mol at the SPMRMP2 level. As well, this pathway shows a small, 1.5 kcal/mol basis set energy difference. Even though the NOCI and T2 cutoffs do not indicate a multireference situation, this reaction involves multiple bond changes, and the dominant NOCI weight is 0.92 for the TS.

The CR-CC(2,3) TS optimization also failed for this reaction. So, the CR-CC(2,3) select forward (reverse) barrier is 77.9 (32.6) kcal/mol. SPMRMP2 forward (reverse) barrier lies 1.0 (8.8) kcal/mol shallower than the corresponding Nguyen barrier while CR-CC(2,3)/aug-cc-pVTZ select forward (reverse) barrier lies 2.1 kcal/mol deeper (3.3 kcal/mol shallower) than the corresponding Nguyen barrier.

3.12 Pathway 24: $CH_2CHOH \rightarrow H_2CCO + H_2$

For this hydrogen dissociation from vinyl alcohol, a (10,10) CAS has two CH σ orbitals farthest from the oxygen in the core as a compromise and also has IOC. The reaction stationary points all have C_s symmetry with an A′ state. However, the CCO angle in H_2CCO slightly bends at the

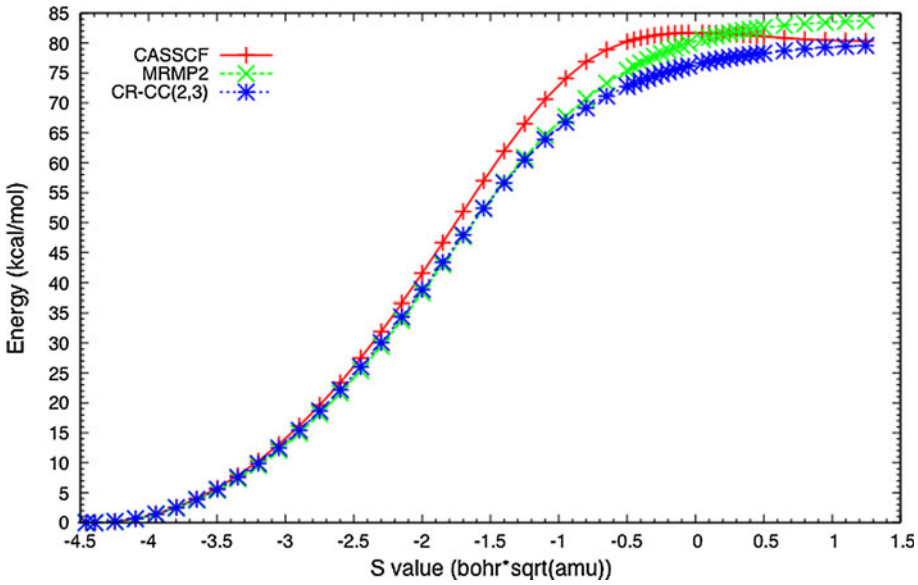

Fig. 2 Path 22 Step 1: CASSCF IRC and single-point energies (aug-cc-pVTZ basis no ZPE)

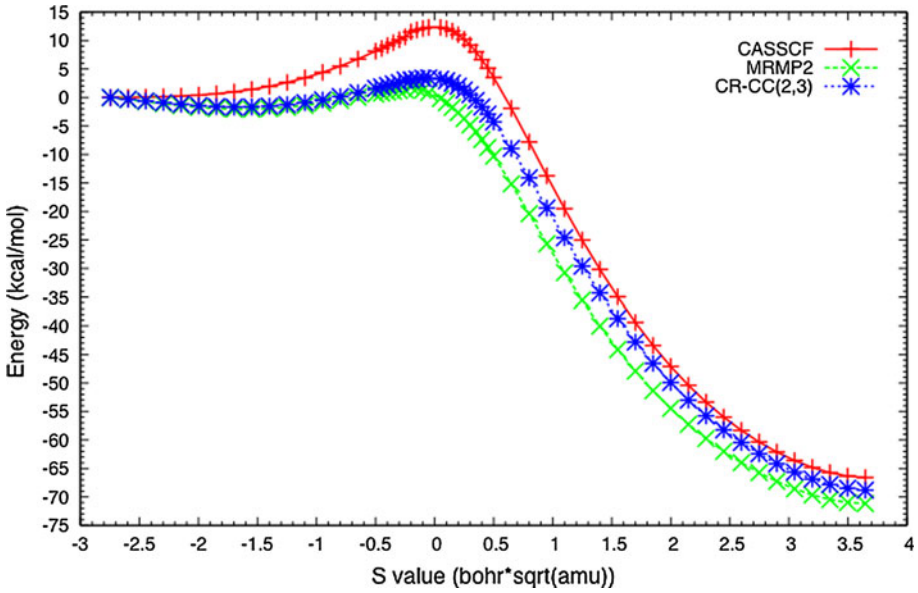

Fig. 3 Path 22 Step 2: CASSCF IRC and single-point energies (aug-cc-pVTZ basis no ZPE)

$\sim$4 Å product end. From our previous study [2], pathway 20 also has this common minimum but does not suffer from this bent angle with a (12,12) CAS. Furthermore, this part of the surface tends to be very flat, which makes optimization difficult. Thus, this bimolecular $\sim$4 Å geometry was pulled out to $\sim$10 Å and asymmetrically re-optimized to avoid this issue. Comparing the $\sim$10 Å and the geometry at the end of the IRC gives less than 1 kcal/mol change in the CASSCF energy. In this case, MRMP2 gives a horizontal shift for the bimolecular $\sim$4 Å product. The forward barrier (reverse barrier) is 84.4 (68.3) kcal/mol at the SPMRMP2 level. Furthermore, the CR-CC(2,3) optimizations led to a forward (reverse) barrier of 85.6 (68.2) kcal/mol. This forward barrier matches the Nguyen forward barrier within 1.0 kcal/mol and the SPMRMP2 barrier within 1.2 kcal/mol. The reverse barrier matches the SPMRMP2 barrier within 1.0 kcal/mol but lies 2.4 kcal/mol shallower than the Nguyen reverse barrier.

3.13 Pathway 25: CH_3C:–OH $\rightarrow$ $H_2CCO + H_2$

This hydrogen molecular dissociation presents a challenge to multireference calculations. After initial calculations with various CAS sizes from Nguyen's starting saddle point geometry, a (12,12) CAS provides a compromised solution where two out of the three, degenerate CH σ orbitals at the unimolecular intermediate remain in the MCSCF core throughout the saddle point search. However, such a search resulted in an unexpected saddle point geometry, or TS 25 (Fig. 4). In addition, the CR-CC(2,3)

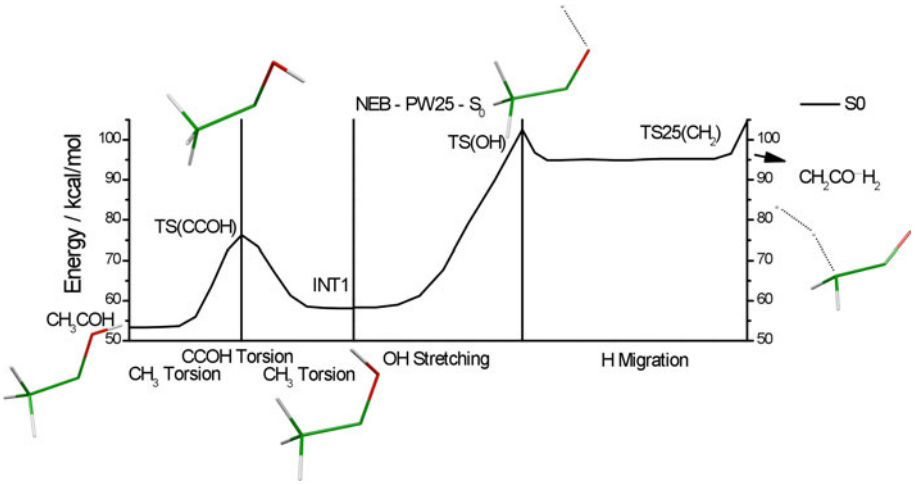

Fig. 4 Non-traditional MEP for pathway 25 shown at the GVB-PP level with a cc-pVDZ basis. The plot displays several TSs between the desired minima

TS optimization failed, and the dominant NOCI weight is 0.84. Another NOCI weight is 0.08, and an occupation number of 0.21 is found, which possibly indicates some multireference character. In order to further characterize this PES region, GVB-PP calculations with the NEB method provided a non-traditional MEP that involves several TSs. Figure 4 displays the NEB results; the potential near TS 25 is particularly flat at the GVB-PP level of theory. Here, the non-traditional MEP between the reactants and products involves three saddle points, and the surface flatness makes location of the minima between these saddle points very difficult. In order to determine the effect of dynamic correlation on this path, stationary points were located at the MR-AQCC level of theory with a cc-pVDZ basis. As a result of the flat surface, TS 25 strongly depends on the presence or absence of dynamic correlation. In particular, the OH distance is 3.76 Å at the GVB-PP level, whereas the same OH distance is 1.95 Å at the MR-AQCC level. Table 4 gives the forward barrier to TS OH at the GVB-PP level and TS 25 at the MR-AQCC level. The forward barrier is 46.8 kcal/mol and 33.0 kcal/mol at the GVB-PP and MR-AQCC levels, respectively.

The most noticeable geometry difference between these structures and Nguyen's saddle point geometry lies in the HH distance. The TS OH geometry most resembles Nguyen's saddle point; however, GVB-PP (MR-AQCC) level of theory yields an HH distance of 2.16 (2.01) Å, whereas Nguyen reported 1.08 Å. As well, the MR-AQCC TS 25 geometry gives a more comparable HH distance of 1.15 Å, but as already noted above, the OH distance differs from Nguyen's reported geometry. Overall, dynamic correlation is as important as quasi-degenerate correlation for determining an accurate, TS geometry in this case.

3.14 Pathway 26: oxirane → ··CH_2 + H_2CO

For this pathway, a (6,6) CAS provides the IRC, which has C_s symmetry throughout the forward barrier and most of the reverse barrier. For the energetics with respect to the basis set, this pathway shows a large 4.6 kcal/mol basis set energy difference. Including dynamic correlation at the SPMRMP2 level leads to a barrierless reaction with an energy gain of 81.4 kcal/mol. Including more correlation with CC-CR(2,3)/aug-cc-pVDZ doublet optimizations resulted in an energy difference of 79.6 kcal/mol. Based on the above basis set energy difference, the energy difference could approximately vary toward 84.2 kcal/mol, which is similar to the Nguyen's result of 85.7 kcal/mol. However, SPMRMP2/aug-cc-pVTZ single-point energy results agree more with the CR-CC(2,3)/aug-cc-pVDZ optimization results than the Nguyen results. No major differences exist in the fragmented geometries. The CASSCF has a potential well on the product side at ~3 Å separation (reaching this symmetric product requires a rotation of the formaldehyde with respect to the methylene, which breaks the original pathway symmetry). The SPMRMP2 reaction enthalpy of 81.4 kcal/mol is within 1.3 kcal/mol of the experimental enthalpy of 80.1 kcal/mol [71–73].

4 Conclusions

In this work, selected pathways of the $O(^1D) + C_2H_4$ PES were calculated at the CASSCF, MRMP2, and CR-CC(2,3) levels of theory. Whenever possible, CASSCF active spaces for pure states did not contain lone O2p orbitals, which tend to lead to IOC ORF with the current, convergence techniques. This active space construction is particularly important in both solving for pure states at the CASSCF level (avoiding IOC ORF) and obtaining single-state MRMP2 results (avoiding state root flipping). In addition, dynamic correlation is also essential for obtaining reasonable energetics—horizontal shifts in the locations of TSs and minima using single-point energetics are small for the singlet reactions in this study. The MRMP2 treatment

captures a significant portion of this correlation but certainly does not encapsulate all of it. In most cases considered here, CR-CC(2,3) results recover additional correlation missed by MRMP2, but in some cases, these coupled cluster results appear to be inappropriate as indicated by the NOCI coefficients. Nonetheless, given comparisons of CR-CC(2,3) single-point data to both Nguyen and experiment, CR-CC(2,3) optimized barriers appear to be crucial for accurate energetics. Furthermore, CR-CC(2,3) TS optimizations sometimes fail for multiple bond changes in some reactions, for which NOCI expansions sometimes suggest multireference character. For a variety of reasons, paths 14, 16, 21, 23, and 25 were computationally difficult. These cases and the cases with a possibly insufficient, double zeta basis in the CR-CC(2,3) calculations limit valid conclusions.

Comparing this work's enthalpies with those available from experiment gives reasonable agreement in many cases. In these reactions, the calculated enthalpy errors range from less than 2.5 kcal/mol to a single, worst case of 6.2 kcal/mol. However, in one case (i.e. pathway 21), our results compare well with Nguyen et al. Future work on O + ethylene will take a number of directions that include further GVB-PP and MR-AQCC energetics with eventual applications toward dynamics for this system.

Acknowledgments The authors are indebted to Michael W. Schmidt and Mark S. Gordon for help in using the capabilities of GAMESS and MCSCF. This material is based upon work supported by the National Science Foundation under Grant No. OISE-0730114 for the Partnerships in International Research and Education (PIRE) and by the Robert A. Welch Foundation under Grant No. D-0005. TeraGrid resources were provided by the Texas Advanced Computing Center (TACC). Support was also provided by the High-Performance Computing Center (HPCC) at Texas Tech University, under the direction of Philip W. Smith. In addition, this work was supported by the Austrian Science Fund within the framework of the Special Research Program F41 (Vienna Computational Materials Laboratory (ViCoM)). Computer time at the Vienna Scientific Cluster (project no. 70019) is gratefully acknowledged. TLW acknowledges computing resources purchased through funds provided by Ames Laboratory and Iowa State University.

References

1. West AC, Kretchmer JS, Sellner B, Park K, Hase WL, Lischka H, Windus TL (2009) O(3P) + C2H4 potential energy surface: study at the multireference level. J Phys Chem A 113(45):12663
2. West AC, Lynch JD, Sellner B, Lischka H, Hase WL, Windus TL (2012) O + C2H4 potential energy surface: excited states and biradicals at the multireference level. Theor Chem Acc 131:1123
3. Casavecchia P, Capozza G, Segoloni E, Leonori F, Balucani N, Volpi Gian G (2005) Dynamics of the O(3P) + C2H4 reaction: identification of five primary product channels (vinoxy, acetyl, methyl, methylene, and ketene) and branching ratios by the crossed molecular beam technique with soft electron ionization. J Phys Chem A 109(16):3527
4. Su H, Zhao S, Liu K, Xiang T (2007) The reactions of O(3P) with terminal alkenes: the H2CO channel via 3,2 H-atom shift. J Phys Chem A 111(38):9600
5. Lee S-H, Huang W-J, Chen W-K (2007) Dynamics of the reaction of atomic oxygen with ethene: observation of all carbon-containing products by single-photon ionization. Chem Phys Lett 446(4–6):276
6. Gardiner WC Jr (ed) (1984) Combustion chemistry. Springer, New York
7. Yamaguchi K, Yabushita S, Fueno T, Kato S, Morokuma K (1980) Geometry optimization of the ring-opened oxirane diradical: mechanism of the addition reaction of the triplet oxygen atom to olefins. Chem Phys Lett 70(1):27
8. Dupuis M, Wendoloski JJ, Takada T, Lester WA Jr (1982) Theoretical study of electrophilic addition: atomic oxygen(3P) + ethylene. J Chem Phys 76(1):481
9. Fueno T, Takahara Y, Yamaguchi K (1990) Approximately projected UHF Moeller-Plesset calculations of the potential energy profiles for the reaction of the triplet oxygen atom with ethylene. Chem Phys Lett 167(4):291
10. Smith BJ, Nguyen Minh T, Bouma WJ, Radom L (1991) Unimolecular rearrangements connecting hydroxyethylidene (CH3-C-OH), acetaldehyde (CH3-CH:O), and vinyl alcohol (CH2:CH-OH). J Am Chem Soc 113(17):6452
11. Jursic BS (1999) Complete basis set ab initio exploring potential energy surface for triplet oxygen reaction with ethylene. THEOCHEM 492:85
12. Nguyen TL, Vereecken L, Hou XJ, Nguyen MT, Peeters J (2005) Potential energy surfaces, product distributions and thermal rate coefficients of the reaction of O(3P) with C2H4(X1Ag): a comprehensive theoretical study. J Phys Chem A 109(33):7489
13. Yang X, Maeda S, Ohno K (2007) Insight into global reaction mechanism of [C2, H4, O] system from ab initio calculations by the Scaled Hypersphere Search Method. J Phys Chem A 111(23):5099
14. Hu W, Lendvay G, Maiti B, Schatz GC (2008) Trajectory surface hopping study of the O(3P) + ethylene reaction dynamics. J Phys Chem A 112(10):2093
15. Joshi A, You X, Barckholtz Timothy A, Wang H (2005) Thermal decomposition of ethylene oxide: potential energy surface, master equation analysis, and detailed kinetic modeling. J Phys Chem A 109(35):8016
16. Shepler BC, Braams BJ, Bowman JM (2008) "Roaming" dynamics in CH3CHO photodissociation revealed on a global potential energy surface. J Phys Chem A 112(39):9344
17. Heazlewood BR, Jordan MJT, Kable SH, Selby TM, Osborn DL, Shepler BC, Braams B, Bowman JM (2008) Roaming is the dominant mechanism for molecular products in acetaldehyde photodissociation. Proc Natl Acad Sci USA Early Ed(Aug 7):1
18. Shepler BC, Braams BJ, Bowman JM (2007) Quasiclassical trajectory calculations of acetaldehyde dissociation on a global potential energy surface indicate significant non-transition state dynamics. J Phys Chem A 111(34):8282
19. Gordon MS, Schmidt MW (2005) Advances in electronic structure theory: GAMESS a decade later. Theory Appl Comput Chem First Forty Years:1167
20. Ruedenberg K, Sundberg KR (1976) MCSCF studies of chemical reactions: natural reaction orbitals and localized reaction orbitals. In: Calais J-L, Goscinski O, Lindenberg J, Öhrn Y (eds) Quantum science. Plenum Publ. Co., New York, pp 505–515
21. Cheung LM, Sundberg KR, Ruedenberg K (1978) Dimerization of carbene to ethylene. J Am Chem Soc 100(25):8024. doi: 10.1021/ja00493a050

22. Cheung LM, Sundberg KR, Ruedenberg K (1979) Electronic rearrangements during chemical reactions. II. Planar dissociation of ethylene. Int J Quantum Chem 16(5):1103. doi:10.1002/qua.560160512
23. Ruedenberg K, Schmidt MW, Gilbert MM (1982) Are atoms intrinsic to molecular electronic wavefunctions? II. Analysis for FORS orbitals. Chem Phys 71(1):51. doi:10.1016/0301-0104(82)87005-5
24. Ruedenberg K, Schmidt MW, Gilbert MM, Elbert ST (1982) Are atoms intrinsic to molecular electronic wavefunctions? III. Analysis of FORS configurations. Chem Phys 71(1):65. doi:10.1016/0301-0104(82)87006-7
25. Ruedenberg K, Schmidt MW, Gilbert MM, Elbert ST (1982) Are atoms intrinsic to molecular electronic wavefunctions? I. The full optimized reaction space (FORS) model. Chem Phys 71(1):41. doi:10.1016/0301-0104(82)87004-3
26. Feller DF, Schmidt MW, Ruedenberg K (1982) Concerted dihydrogen exchange between ethane and ethylene. SCF and FORS calculations of the barrier. J Am Chem Soc 104(4):960. doi:10.1021/ja00368a006
27. Siegbahn P, Heiberg A, Roos B, Levy B (1980) A comparison of the super-CI and the Newton-Raphson scheme in the complete active space SCF method. Phys Scr 21(3–4):323. doi:10.1088/0031-8949/21/3-4/014
28. Roos B (1987) The complete active space self-consistent field method and its applications in electronic structure calculations. Adv Chem Phys Ab Initio Method Quantum Chem, part 2 69:399–455
29. Roos BO (1992) The multiconfigurational (MC) self-consistent field (SCF) theory. In: Malmqvist PA, Olsen J, Taylor PR, Roos BO, Siegbahn PEM, Helgaker T, Wahlgren U (eds) Lecture notes in quantum chemistry. European summer school in quantum chemistry, lecture notes in chemistry, vol 58. Springer-Verlag, Berlin, pp 177–200
30. Dunning TH Jr (1989) Gaussian basis sets for use in correlated molecular calculations. I. The atoms boron through neon and hydrogen. J Chem Phys 90(2):1007
31. Ivanic J, Ruedenberg K (2001) Identification of deadwood in configuration spaces through general direct configuration interaction. Theor Chem Acc 106(5):339
32. Lengsfield BH III (1980) General second order MCSCF theory: a density matrix directed algorithm. J Chem Phys 73:382
33. Fletcher GD (2007) A parallel multi-configuration self-consistent field algorithm. Mol Phys 105(23–24):2971
34. Yarkony DR (1981) Comment on the use of augmented Matrix in MCSCF Theory. Chem Phys Lett 77(3):634
35. Bauschlicher CW Jr (1980) The construction of modified virtual orbitals (MVO's) which are suited for configuration interaction calculations. J Chem Phys 72(2):880
36. Boys SF (1966) Localized orbitals and localized adjustment functions. In: Lödin P-O (ed) Quantum theory of atoms, molecules, and the solid state. A tribute to John C. Slater. Academic Press, New York, pp 253–261
37. Gonzalez C, Schlegel HB (1989) An improved algorithm for reaction path following. J Chem Phys 90(4):2154
38. Hirao K (1992) Multireference Moeller-Plesset method. Chem Phys Lett 190(3–4):374
39. Szalay PG, Bartlett RJ (1993) Multireference averaged quadratic coupled-cluster method: a size-extensive modification of multireference CI. Chem Phys Lett 214(5):481
40. Lischka H, Shepard R, Brown FB, Shavitt I (1981) New implementation of the graphical unitary group approach for multireference direct configuration interaction calculations. Int J Quantum Chem Quantum Chem Symp 15:91
41. Lischka H, Shepard R, Pitzer RM, Shavitt I, Dallos M, Muller T, Szalay PG, Seth M, Kedziora GS, Yabushita S, Zhang Z (2001) High-level multireference methods in the quantum-chemistry program system COLUMBUS: analytic MR-CISD and MR-AQCC gradients and MR-AQCC-LRT for excited states, GUGA spin-orbit CI and parallel CI density. Phys Chem Chem Phys 3(5):664
42. Lischka H, Shepard R, Shavitt I, Pitzer RM, Dallos M, Mueller T, Szalay PG, Brown FB, Ahlrichs R, Boehm HJ, Chang A, Comeau DC, Gdanitz R, Dachsel H, Ehrhardt C, Ernzerhof M, Hoechtl P, Irle S, Kedziora G, Kovar T, Parasuk V, Pepper MJM, Scharf P, Schiffer H, Schindler M, Schueler M, Seth M, Stahlberg EA, Zhao J-G, Yabushita S, Zhang Z, Barbatti M, Matsika S, Schuurmann M, Yarkony DR, Brozell SR, Beck EV, Blaudeau J-P, Ruckenbauer M, Sellner B, Plasser M, Szymczak JJ (2010) COLUMBUS, an ab initio electronic structure program, release 5.9.2. www.univie.ac.at/columbus
43. Piecuch P, Kucharski SA, Kowalski K, Musial M (2002) Efficient computer implementation of the renormalized coupled-cluster methods: the R-CCSD[T], R-CCSD(T), CR-CCSD[T], and CR-CCSD(T) approaches. Comput Phys Commun 149(2):71
44. Piecuch P, Wloch M (2005) Renormalized coupled-cluster methods exploiting left eigenstates of the similarity-transformed Hamiltonian. J Chem Phys 123(22):224105/1
45. Hay PJ, Hunt WJ, Goddard WA III (1972) Generalized valence bond description of simple alkanes, ethylene, and acetylene. J Amer Chem Soc 94(24):8293
46. Hunt WJ, Hay PJ, Goddard WA III (1972) J Chem Phys 57:738
47. Shepard R, Kedziora GS, Lischka H, Shavitt I, Mueller T, Szalay PG, Kallay M, Seth M (2008) The accuracy of molecular bond lengths computed by multireference electronic structure methods. Chem Phys 349(1–3):37
48. Bunge AV (1970) Electronic wavefunctions for atoms. III. Partition of degenerate spaces and ground state of carbon. J Chem Phys 53(1):20
49. Pulay P, Fogarasi G, Pongor G, Boggs JE, Vargha A (1983) Combination of theoretical ab initio and experimental information to obtain reliable harmonic force constants. Scaled quantum mechanical (QM) force fields for glyoxal, acrolein, butadiene, formaldehyde, and ethylene. J Am Chem Soc 105(24):7037
50. Shepard R (1995) The analytic gradient method for configuration interaction wave functions. Adv Ser Phys Chem 2(Modern Electronic Structure Theory, Pt. 1):345–358
51. Shepard R, Lischka H, Szalay PG, Kovar T, Ernzerhof M (1992) A general multireference configuration interaction gradient program. J Chem Phys 96(3):2085
52. Lischka H, Dallos M, Shepard R (2002) Analytic MRCI gradient for excited states: formalism and application to the n-pi valence- and n-(3 s,3p) Rydberg states of formaldehyde. Mol Phys 100(11):1647
53. Mills G, Jonsson H (1994) Quantum and thermal effects in H2 dissociative adsorption: evaluation of free energy barriers in multidimensional quantum systems. Phys Rev Lett 72(7):1124
54. Mills G, Jonsson H, Schenter GK (1995) Reversible work transition state theory: application to dissociative adsorption of hydrogen. Surf Sci 324(2/3):305
55. Henkelman G, Jonsson H (2000) Improved tangent estimate in the nudged elastic band method for finding minimum energy paths and saddle points. J Chem Phys 113(22):9978
56. Gonzalez-Garcia N, Pu J, Gonzalez-Lafont A, Lluch JM, Truhlar DG (2006) Searching for saddle points by using the nudged elastic band method: an implementation for gas-phase systems. J Chem Theory Comput 2(4):895. doi:10.1021/ct060032y
57. Anglada JM, Bofill JM (1997) A reduced-restricted-quasi-Newton-Raphson method for locating and optimizing energy crossing points between two potential energy surfaces. J Comput Chem 18(8):992
58. Fukui K (1970) Formulation of the reaction coordinate. J Phys Chem 74(23):4161. doi:10.1021/j100717a029

59. Fukui K (1981) The path of chemical reactions: the IRC approach. Acc Chem Res 14(12):363. doi:10.1021/ar00072a001
60. Sellner B (2011) Photochemistry of organic molecules using high-level multireference methods. Dissertation, University of Vienna
61. Chao J, Hall KR, Marsh KN, Wilhoit RC (1986) Thermodynamic properties of key organic oxygen compounds in the carbon range C1 to C4. Part 2. Ideal gas properties. J Phys Chem Ref 15(4):1369
62. Holmes JL, Lossing FP (1982) Heats of formation of ionic and neutral enols of acetaldehyde and acetone. J Am Chem Soc 104(9):2648
63. Tsang W (1996) Heats of formation of organic free radicals by kinetic methods. Struct Energ React Chem Ser 4(Energetics of Organic Free Radicals):22–58
64. Niiranen JT, Gutman D, Krasnoperov LN (1992) Kinetics and thermochemistry of the acetyl radical: study of the acetyl + hydrogen bromide −> acetaldehyde + bromine atom reaction. J Phys Chem 96(14):5881
65. JANAF Thermochemical Tables (1985) National Standard Reference Data Service; US National Bureau of Standards: Washington, p 37
66. Chase MW Jr (1998) NIST-JANAF thermochemical tables 4th ed. J Phys Chem Ref Data. Mongr 9, American Chemical Society, Washington, DC, p 127
67. Becke AD (1993) Density-functional thermochemistry. III. The role of exact exchange. J Chem Phys 98(7):5648. doi:10.1063/1.464913
68. Stephens PJ, Devlin FJ, Chabalowski CF, Frisch MJ (1994) Ab initio calculation of vibrational absorption and circular dichroism spectra using density functional force fields. J Phys Chem 98(45):11623. doi:10.1021/j100096a001
69. Hehre WJ, Ditchfield R, Pople JA (1972) Self-consistent molecular orbital methods. XII. Further extensions of Gaussian-type basis sets for use in molecular orbital studies of organic molecules. J Chem Phys 56(5):2257. doi:10.1063/1.1677527
70. Hariharan PC, Pople JA (1973) Influence of polarization functions on MO hydrogenation energies. Theoret Chim Acta 28(3):213. doi:10.1007/bf00533485
71. Chase MW Jr, Davies CA, Downey JR Jr, Frurip DJ, McDonald RA, Syverud AN (1985) JANAF thermochemical tables (Third Edition). J Phys Chem Ref Data 14(1):1–100
72. Gurvich LVV, Veyts IV, Alcock CB (1989) Thermodynamic properties of individual substances, Fourth Edition. Hemisphere Pub. Co., New York
73. Ruscic BBJ, Burcat A, Csaszar AG, Demaison J, Janoschek R, Martin JML, Morton ML, Rossi MJ, Stanton JF, Szalay PG, Westmoreland PR, Zabel F, Berces T (2005) IUPAC critical evaluation of thermochemical properties of selected radicals. Part I. J Phys Chem Ref Data 34(2):573